A Kinetic and Product Study of the Cl + HO_2 Reaction

Kevin M. Hickson* and Leon F. Keyser

Earth and Space Sciences Division, Jet Propulsion Laboratory, California Institute of Technology, Pasadena, California 91109

Received: March 7, 2005; In Final Form: June 10, 2005

Absolute rate data and product branching ratios for the reactions Cl + HO_2 → HCl + O_2 (k_{1a}) and Cl + HO_2 → OH + ClO (k_{1b}) have been measured from 226 to 336 K at a total pressure of 1 Torr of helium using the discharge flow resonance fluorescence technique coupled with infrared diode laser spectroscopy. For kinetic measurements, pseudo-first-order conditions were used with both reagents in excess in separate experiments. HO_2 was produced by two methods: through the termolecular reaction of H atoms with O_2 and also by the reaction of F atoms with H_2O_2. Cl atoms were produced by a microwave discharge of Cl_2 in He. HO_2 radicals were converted to OH radicals prior to detection by resonance fluorescence at 308 nm. Cl atoms were detected directly at 138 nm also by resonance fluorescence. Measurement of the consumption of HO_2 in excess Cl yielded k_{1a} and measurement of the consumption of Cl in excess HO_2 yielded the total rate coefficient, k_1. Values of k_{1a} and k_1 derived from kinetic experiments expressed in Arrhenius form are $(1.6 \pm 0.2) \times 10^{-11}$ exp[$(249 \pm 34)/T$] and $(2.8 \pm 0.1) \times 10^{-11}$ exp[$(123 \pm 15)/T$] cm^3 $molecule^{-1}$ s^{-1}, respectively. As the expression for k_1 is only weakly temperature dependent, we report a temperature-independent value of $k_1 = (4.5 \pm 0.4) \times 10^{-11}$ cm^3 $molecule^{-1}$ s^{-1}. Additionally, an Arrhenius expression for k_{1b} can also be derived: $k_{1b} = (7.7 \pm 0.8) \times 10^{-11}$ exp[$-(708 \pm 29)/T$] cm^3 $molecule^{-1}$ s^{-1}. These expressions for k_{1a} and k_{1b} are valid for 226 K ≤ T ≤ 336 and 256 K ≤ T ≤ 296 K, respectively. The cited errors are at the level of a single standard deviation. For the product measurements, an excess of Cl was added to known concentrations of HO_2 and the reaction was allowed to reach completion. HCl product concentrations were determined by IR absorption yielding the ratio k_{1a}/k_1 over the temperature range 236 K ≤ T ≤ 296 K. OH product concentrations were determined by resonance fluorescence giving rise to the ratio k_{1b}/k_1 over the temperature range 226 K ≤ T ≤ 336 K. Both of these ratios were subsequently converted to absolute numbers. Values of k_{1a} and k_{1b} from the product experiments expressed in Arrhenius form are $(1.5 \pm 0.1) \times 10^{-11}$ exp[$(222 \pm 17)/T$] and $(10.6 \pm 1.5) \times 10^{-11}$ exp[$-(733 \pm 41)/T$] cm^3 $molecule^{-1}$ s^{-1}, respectively. These expressions for k_{1a} and k_{1b} are valid for 256 K ≤ T ≤ 296 and 226 K ≤ T ≤ 336 K, respectively. A combination of the kinetic and product data results in the following Arrhenius expressions for k_{1a} and k_{1b} of $(1.4 \pm 0.3) \times 10^{-11}$ exp[$(269 \pm 58)/T$] and $(12.7 \pm 4.1) \times 10^{-11}$ exp[$-(801 \pm 94)/T$] cm^3 $molecule^{-1}$ s^{-1}, respectively. Numerical simulations were used to check for interferences from secondary chemistry in both the kinetic and product experiments and also to quantify the losses incurred during the conversion process HO_2 → OH for detection purposes.

Introduction

The reaction of atomic chlorine, Cl, with the hydroperoxy radical, HO_2, plays a significant role in chlorine partitioning in the stratosphere. Reaction 1a is particularly important for the conversion of active chlorine containing species (Cl and ClO) to inactive HCl at altitudes of 30 km and higher.

$$Cl + HO_2 \rightarrow HCl + O_2 \qquad \Delta H = -(54.4 \pm 0.8) \text{ kcal mol}^{-1} \quad (1a)$$

$$Cl + HO_2 \rightarrow OH + ClO \qquad \Delta H = (0.9 \pm 0.8) \text{ kcal mol}^{-1} \quad (1b)$$

Above 40 km, reaction 1a is thought to produce HCl in significant quantities compared with the reactions of Cl with methane and of OH with ClO, the major sources of HCl at these altitudes. The fraction of Cl that is converted through reaction 1b to ClO, however, has not been well determined by previous work. Several earlier studies have been performed to better understand the kinetics of reaction 1. These studies consist of measurements of the total rate coefficient, k_1, and of the minor channel rate coefficient, k_{1b}, by relative rate (indirect) methods,[1−4] via fits to a complex mechanism,[5,6] or through absolute measurements.[7−9] The relative rate studies used the techniques of discharge-flow coupled with mass spectrometric detection[1,2]/laser magnetic resonance[3] or flash photolysis coupled with UV absorption spectroscopy.[4] The studies involving complex mechanisms used flash photolysis coupled with UV absorption spectroscopy.[5,6] These studies obtained values for k_1 which range from $(1.9-6.8) \times 10^{-11}$ cm^3 $molecule^{-1}$ s^{-1}. There are three previous absolute determinations of the kinetics of reaction 1. The earliest, by Lee and Howard,[7] was undertaken using a discharge-flow technique coupled with laser magnetic resonance detection of HO_2, OH, and ClO. Chlorine atom concentrations were determined by titration with O_3 and were subsequently detected as ClO. Under pseudo-first-order conditions with Cl

* To whom correspondence should be addressed. Fax: (818) 393-5019. E-mail: kevin.hickson@jpl.nasa.gov.

10.1021/jp051176w CCC: $30.25
Published on Web 07/19/2005

as the excess reagent, they reported a temperature-independent value for $k_1 = (4.2 \pm 0.7) \times 10^{-11}$ cm^3 molecule^{-1} s^{-1} from 250 to 420 K. A later study by Dobis and Benson[8] used a very low-pressure reactor (VLPR) coupled with mass spectrometric detection to determine k_1. They obtained $k_1 = (4.45 \pm 0.06) \times 10^{-11}$ cm^3 molecule^{-1} s^{-1} also independent of temperature in the range $T = 243-368$ K. The most recent and the most complete study of the reaction of Cl with HO_2 by Riffault et al.[9] used a discharge-flow technique combined with mass spectrometric detection. They followed the pseudo-first-order kinetics of Cl consumption in excess HO_2 and of HO_2 consumption in excess Cl to determine a weakly negative temperature dependence for k_1. Considering the experimental uncertainty, they quote a temperature-independent value for k_1 of $(4.4 \pm 0.6) \times 10^{-11}$ cm^3 molecule^{-1} s^{-1} from 230 to 360 K.

Despite the apparent agreement for the value of k_1 between previous studies, the fraction of the reaction that proceeds through channel 1b is not well established. Burrows et al.[3] looked for the production of OH radicals in an attempt to determine the branching ratio k_{1b}/k_1. OH radicals were not observed, which led the authors to publish an upper limit of $k_{1b} \leq 3 \times 10^{-13}$ cm^3 molecule^{-1} s^{-1}, which yielded a small branching fraction for $k_{1b}/k_1(298\text{K}) \leq 0.008$. Dobis and Benson[8] also reported a small value for $k_{1b}/k_1 = (0.05 \pm 0.03)$ over the temperature range 243−368 K. Lee and Howard[7] observed the production of both OH and ClO from reaction 1b and reported an expression for $k_{1b}/k_1 = (1.09 \pm 0.06) \exp[-(478 \pm 17)/T]$, which gave $k_{1b}/k_1(298\text{K}) = 0.22$. Similarly, Cattell and Cox[6] reported $k_1 = 4.4 \times 10^{-11}$ cm^3 molecule^{-1} s^{-1} and $k_{1b} = 9.4 \times 10^{-12}$ cm^3 molecule^{-1} s^{-1}, which gave rise to a value for $k_{1b}/k_1(308\text{K}) = 0.18$. Finally, Riffault et al.[9] observed the time evolution of OH and ClO formed in reaction 1b and subsequently fitted these profiles by varying the input parameters, k_1 and k_{1b}/k_1. The best fit to the data was obtained for a value of $k_{1b}/k_1(298\text{K}) = (0.22 \pm 0.01)$. The available data for the branching fraction k_{1b}/k_1 range between 0 and 0.22 at 298 K and it is clear that further study of this quantity is required. Apart from its importance to stratospheric modeling, an accurate determination of k_{1b} would be useful for the calculation of the enthalpy of formation of HO_2. By coupling the experimentally determined Arrhenius expression for reaction 1b with the Arrhenius expression for reaction 2a,

$$OH + ClO \rightarrow Cl + HO_2 \quad (2a)$$

$$\rightarrow HCl + O_2 \quad (2b)$$

we can obtain a value for the reaction enthalpy, ΔH_r, by using the van't Hoff equation. The enthalpy of formation of HO_2, $\Delta H_{f,298K}(HO_2)$, can subsequently be determined using Hess' law.[10] Current evaluations[11,12] of the available data for reaction 1 used in stratospheric modeling are either based upon the results of Lee and Howard[7] alone[11] over the temperature range 250 to 420 K or upon the results of Lee and Howard[7] and Riffault et al.[9] together[12] over the temperature range 230 to 420 K. The former evaluation recommends a temperature-independent value for k_1 of $(4.2 \pm 0.7) \times 10^{-11}$ cm^3 molecule^{-1} s^{-1}. The latter adopts a value of 4.3×10^{-11} cm^3 molecule^{-1} s^{-1}.

The present study, using a discharge-flow, resonance-fluorescence technique coupled with tunable diode laser absorption for HCl detection, has been undertaken to provide kinetic and product data for reaction 1. Specifically, kinetic data have been recorded by monitoring the kinetics of both Cl and HO_2 at temperatures ranging from 226 to 336 K. Product data have been taken by measuring HCl produced by reaction 1a and OH produced by reaction 1b under conditions of excess Cl at temperatures also ranging from 226 to 336 K.

Experimental Section

The flow system used in the present study is essentially that described in a recent paper in detail.[13]

Reactor. The main reaction vessel was constructed from Pyrex and has an internal diameter of 5.04 cm and is 62 cm in length. The downstream end of the vessel was connected to an octagonal stainless steel resonance fluorescence cell. The gas pressure was measured via a 10 Torr capacitance manometer that was attached to the system between the resonance fluorescence cell and the reactor. At the upstream end of the reactor were connections to either a fixed HO_2 source and a moveable Cl inlet, or a moveable HO_2 source and a fixed Cl inlet depending upon the desired configuration. These sources are described in more detail below. The inner surface of the reaction vessel and the inner and outer surfaces of the moveable inlet were coated with halocarbon wax (Series 15-00, Halocarbon Corp.) to minimize heterogeneous radical loss. The carrier gas used in all experiments was helium, at a total flow rate of approximately 2300 to 2800 sccm (std atm cm^3 min^{-1}), which allowed total flow velocities ranging from 1400 to 2100 cm s^{-1}. Measurements were made at temperatures ranging from 226 to 336 K. The flow system was evacuated by a 38 L s^{-1} rotary pump and a throttling valve was used to maintain the pressure at approximately 1 Torr. Temperatures in the reaction zone were maintained to within ±2 K using a temperature-controlled bath (Neslab, ULT-80DD or RTE-100) that circulated a given fluid (methanol or water) through the external jacket of the reactor. Two thermocouples (Type E, chromel−constantan) were used to monitor the fluid temperature inside the jacket, one at either end of the reaction vessel.

HO_2 Source. HO_2 was generated by one of two methods during the course of this study. The first method, to produce a low concentration of HO_2 radicals ($\leq 5 \times 10^{10}$ molecules cm^{-3}) for experiments in excess Cl atoms, utilized the reaction

$$H + O_2 + M \rightarrow HO_2 + M \quad (3)$$

with M being He, the carrier gas. H atoms were produced in a 2.45 GHz discharge (60 W) of a dilute mixture of H_2/He in a quartz tube and were subsequently further diluted with a larger flow of He through the discharge. Total flow rates of He through the discharge were approximately 1700 sccm. The output of the discharge was mixed with a flow of approximately 550 sccm of O_2 in a region coated with halocarbon wax to prevent radical losses. This flow corresponded to concentrations of O_2 in the flow tube in the range $(6-8) \times 10^{15}$ molecules cm^{-3}. This region, 19 cm long with an internal cross-section of 2.5 cm^2, was attached to a sideport upstream of the main reactor and was maintained at a pressure of approximately 20 Torr to drive the three-body formation of HO_2 through reaction 3. Flow velocities in this pre-reactor were calculated to be of the order of 620 cm s^{-1} giving a residence time of approximately 31 ms. Using $k_3 = 5.8 \times 10^{-32}$ cm^6 molecule^{-2} s^{-1},[11] we calculate that the $H + O_2$ reaction was sufficiently fast to prevent any H atoms from entering the main reaction vessel. By this method, HO_2 concentrations in the flow tube could be produced in the range $(0.3-7.0) \times 10^{10}$ molecules cm^{-3}.

The second method, to produce a high concentration of HO_2 radicals (up to 4×10^{12} molecules cm^{-3}) for experiments in excess HO_2, utilized the reaction

$$F + H_2O_2 \rightarrow HF + HO_2 \quad (4)$$

$$k_4(300K) = 5.0 \times 10^{-11}\ cm^3\ molecule^{-1}\ s^{-1}\ (ref\ 11)$$

F atoms were generated using a 2.45 GHz discharge (20 W) of a dilute mixture of F_2/He in an alumina tube to improve the F_2 dissociation efficiency. The F atoms were subsequently flowed into a moveable inlet at the upstream end of the reaction vessel through an inner injector. H_2O_2 was contained in a temperature-controlled vessel held at 291 K to prevent H_2O_2 condensation further downstream and a small flow of He was bubbled through the H_2O_2 to carry some of the vapor into the outer injector of the moveable inlet. The pressure in the temperature-controlled vessel was kept at approximately 6 Torr. The relative position of the inner injector, which had an internal cross-section of 0.2 cm^2, could be altered such that it was possible to vary the reaction time between F + H_2O_2 to ensure that no F atoms entered the main reactor. The moveable inlet itself was 180 cm long with an internal cross-section of 1.3 cm^2. The total flow through the moveable inlet was approximately 900 sccm such that flow velocities ranging from 3900 to 5400 cm s^{-1} within the inlet were routinely used. All surfaces within the inlet were coated with halocarbon wax. H_2O_2 was purified prior to use by pumping and also by bubbling He through it to remove most of the H_2O impurity. The H_2O_2 purity was estimated to be approximately 96 wt % based on earlier measurements[14] under the same experimental conditions.

HO_2 Detection. HO_2 was not directly detected in these experiments. Instead, HO_2 was first converted to OH by adding a large excess of NO (approximately 2×10^{14} molecules cm^{-3}) to the flow approximately 3 ms upstream from the resonance cell via the reaction

$$HO_2 + NO \rightarrow OH + NO_2 \quad (5)$$

$$k_5(298K) = 8.1 \times 10^{-12}\ cm^3\ molecule^{-1}\ s^{-1}\ (ref\ 11)$$

NO was purified prior to use by passing it through a molecular sieve held at 195 K to remove any potential NO_2 impurity. The OH radicals generated by this titration were subsequently detected by resonance fluorescence. A quartz resonance lamp operated at a microwave power of 60 W was used to excite the OH fluorescence. A stream of helium saturated with water vapor was flowed through the lamp at a pressure of approximately 1.1 Torr. The light was baffled and collimated prior to entering the resonance cell using a series of concentric rings. Wood's horns were placed opposite the lamp and detection system to reduce further the detection of scattered light. The resultant hydroxyl radical fluorescence produced in the illuminated portion of the cell was also baffled with a similar arrangement of rings and observed near 308 nm in the (0, 0) band of the OH ($A^2\Sigma^+ - X^2\Pi$) system using an interference filter (Corion 3100-1) and a photomultiplier tube (EMR 510E) perpendicular to the incident radiation. The output of the PMT was then processed using an amplifier−discriminator (Ortec 9302) and counter−timer system (Stanford Research Systems SR400) which were interfaced to a computer for data acquisition and analysis. The filter used has a transmission of 17% at 308 nm; it was placed between the PMT and a suprasil quartz window which formed a vacuum seal to the flow system. As such, the filter was never in contact with any of the reagents used in the experiments. Typically, photons incident on the PMT were integrated over a 10-s period and then averaged over 5 or 10 iterations. During the experimental runs, background fluorescence signals were recorded with the NO flow through the fixed inlet switched off. During the conversion of HO_2 to OH, some radical loss was expected to occur mainly through the reactions

$$OH + HO_2 \rightarrow H_2O + O_2 \quad (6)$$

$$k_6(298K) = 1.1 \times 10^{-10}\ cm^3\ molecule^{-1}\ s^{-1}\ (ref\ 11)$$

$$OH + OH \rightarrow H_2O + O \quad (7)$$

$$k_7(298K) = 1.9 \times 10^{-12}\ cm^3\ molecule^{-1}\ s^{-1}\ (ref\ 11)$$

$$OH + wall \rightarrow products \quad (8)$$

$$k_8 = experimentally\ determined$$

$$OH + NO + He \rightarrow HONO + He \quad (9)$$

$$k_9(298K) = 7.2 \times 10^{-31}\ cm^6\ molecule^{-2}\ s^{-1}\ (ref\ 11)$$

To estimate the magnitude of radical loss, the HO_2 to OH conversion was simulated with computer models. These losses were calculated to be within the range of 2 to 30% and were found to be approximately 8% on average. The conversion losses were subsequently incorporated into the HO_2 concentration measurements. Concentrations of HO_2 when used as the excess reagent were calculated from the average observed OH fluorescence intensities at the minimum and maximum reaction times of each experimental run. These concentrations differed by up to approximately 8% due to the heterogeneous loss of HO_2 in addition to its gas-phase self-reaction

$$HO_2 + HO_2 \rightarrow H_2O_2 + O_2 \quad (10)$$

$$k_{10}(298K) = 1.7 \times 10^{-12}\ cm^3\ molecule^{-1}\ s^{-1}\ (ref\ 11)$$

OH Detection. Product OH radicals generated by channel 1b were detected in an identical fashion to HO_2 radicals, without the need for initial chemical conversion.

OH Calibration. To accurately determine HO_2 concentrations, it was necessary to know the absolute OH concentrations generated by titration with NO. As such, a calibration of the OH resonance fluorescence lamp was performed on a daily basis to determine its detection sensitivity. The system was calibrated by forming specific amounts of OH radicals from the reaction of a known flow of NO_2 and an excess of H atoms

$$H + NO_2 \rightarrow OH + NO \quad (11)$$

$$k_{11}(298K) = 1.3 \times 10^{-10}\ cm^3\ molecule^{-1}\ s^{-1}\ (ref\ 11)$$

H atoms were generated as described above, upstream of the main reactor in a fixed side port. A flow of a known composition of NO_2 in helium was added to the main flow through the moveable inlet. The OH signal intensity was recorded and then the procedure was repeated for different flows of NO_2. A plot of NO_2 concentration (which was assumed to be converted to OH at 100% efficiency) against signal intensity was linear at OH concentrations lower than 4×10^{12} molecule cm^{-3}, the gradient of which yielded the OH detector sensitivity, S_{OH}. Calibrations were carried out at each temperature used in the experiments although no temperature dependence of the OH sensitivity was observed. Typically, OH count rates varied from 30 cts s^{-1} (for OH product measurements) to 1.2×10^5 cts s^{-1} (for experiments with HO_2 in excess). At a typical lamp sensitivity of 3×10^{-8} cts s^{-1}/molecule cm^{-3} these count rates

TABLE 1: Summary of Radical Wall Loss Rates[a]

T/K	OH wall loss rate coefficient/s^{-1}	HO_2 wall loss rate coefficient/s^{-1}	Cl atom wall loss rate coefficient/s^{-1}
336		6.8 ± 2.1	2.9 ± 1.7
316		7.9 ± 1.8	2.9 ± 2.1
296	2.1 ± 0.5	7.6 ± 2.4	2.5 ± 1.4
276	5.6 ± 0.5	4.8 ± 2.7	2.1 ± 1.7
256	7.1 ± 1.0	7.8 ± 3.9	5.1 ± 2.7
236	9.5 ± 0.4	3.8 ± 1.4	4.6 ± 3.0
226	14.5 ± 0.5	4.6 ± 1.2	5.6 ± 3.2

[a] Errors are cited at the level of a single standard deviation.

corresponded to OH concentrations ranging from 1×10^9 to 4×10^{12} molecule cm^{-3}. Typical background signals were near 250 cts s^{-1}, and for the 50 s counting times used, a minimum detectable OH concentration of 1×10^8 molecule cm^{-3} at a signal-to-noise ratio of unity could be observed.

OH and HO_2 Wall Losses. OH radicals were generated as a product of the minor channel of the Cl + HO_2 reaction. Consequently, it was important to determine the heterogeneous losses of OH to correct the OH product concentrations if necessary. OH radicals were also produced as a method for HO_2 detection as described above. The losses of OH radicals on the walls of the main reactor were measured by generating OH radicals at the tip of the moveable inlet via the reaction of H atoms with an excess of NO_2 (reaction 1) at different reaction times. Thus a plot of the log of the intensity of the OH fluorescence signal versus reaction time yielded the pseudo-first-order loss rate for OH at the temperature of measurement. The measurements were repeated at all temperatures used during the course of the experiments and are presented in Table 1. These values contain a correction for the diffusional loss of OH radicals.

HO_2 wall losses prior to conversion to OH also needed to be considered. These loss rates were not measured directly, but were taken to be the intercepts of the second-order plots of the loss of HO_2 radicals in the presence of excess Cl. The measured wall loss rates after corrections for the diffusional loss of HO_2 have been made are presented in Table 1.

Cl Source. Cl atoms were generated in both sets of experiments using a 2.45 GHz discharge at 60 W of a dilute mixture of Cl_2/He in a Suprasil quartz tube, either in the moveable inlet or in the fixed side port depending on the experimental method used. The walls of the tube were coated with phosphoric acid immediately downstream of the discharge to minimize the loss of Cl through heterogeneous recombination. Dissociation efficiencies were found to be on the order of 15% for typical Cl atom concentrations ranging from 2×10^{10} to 3×10^{12} molecule cm^{-3}.

Cl Detection. Relative intensities of atomic chlorine emission were observed in the resonance fluorescence cell downstream from the temperature-controlled portion of the flow system. Atomic chlorine fluorescence was excited by radiation from a 60 W microwave discharge in a resonance lamp. A mixture of approximately 0.13% Cl_2 in He was passed through the lamp at a total pressure of approximately 1.5 Torr. Light emitted from the lamp was collimated using a series of concentric baffles, before entering the resonance cell. Fluorescence was emitted from the atomic chlorine within the illuminated portion of the cell on-resonance with the exciting radiation, mainly in the $(4s^1 3p^4)^4P_{3/2} \rightarrow (3p^5)^2P_{3/2}$ transition at 137.96 nm. The fluorescence was observed perpendicular to the incident radiation using a channel photomultiplier (CPM) (Perkin-Elmer 1911P) which was sensitive to light between 120 and 200 nm. Immediately in front of the CPM, a 1 mm thick BaF_2 window was used as a cut-on filter to eliminate possible interference from oxygen and hydrogen atom emission. It was thought that this might potentially result from impurities in some of the gas flows. A second series of baffles was used in front of this window and Wood's horns were placed opposite the lamp and CPM to reduce further the detection of scattered light. The CPM output signal was passed to a photon counting system (Stanford Research Systems SR400) where typically signals were integrated for 10 s and averaged over 5 iterations. During the experimental runs, background fluorescence signals were recorded with the Cl_2 flow through the fixed inlet switched off.

Cl Calibration. To accurately determine Cl atom concentrations, in particular for experiments where Cl atoms were used as the excess reagent, it was important to calibrate the chlorine atom concentrations on a daily basis. The sensitivity of the detection system to Cl atom concentrations in the flow cell was determined by generating a known concentration of Cl atoms via the reaction of excess F atoms with Cl_2

$$F + Cl_2 \rightarrow Cl + FCl \qquad (12)$$

$$k_{12}(298K) = 1.6 \times 10^{-10}\ cm^3\ molecule^{-1}\ s^{-1}\ (ref\ 11)$$

F atoms were produced in a microwave discharge of a 0.5% mixture of F_2 in helium in a fixed port upstream of the main reactor. An uncoated 1 cm i.d. alumina tube was used in the microwave source, which was operated at 20 W. Typical flow rates through the discharge were on the order of 600 sccm. Background signals which consisted of scattered light and light from secondary sources of Cl atoms were determined by simply turning off the Cl_2 flow through the microwave discharge. Calibrations were performed under similar flow conditions to those used in the experiments. It was discovered that when O_2 was added to the system for the generation of HO_2 radicals by reaction 3, the sensitivity to Cl was reduced by a significant amount probably due to absorption of lamp light. As such, all calibrations for experiments of this type were performed with the same concentration of O_2 present. Typical detection sensitivities were found to be in the region of 2×10^{-6} cts s^{-1}/atoms cm^{-3} with background signals at about 5000 cts s^{-1} for Cl atom concentrations less than approximately 2×10^{11} atoms cm^{-3}. For a 50 s counting time, this was equivalent to a minimum detectable Cl atom concentration of 7×10^6 atoms cm^{-3} at a signal-to-noise ratio of unity. For higher concentrations, such as when the experiments were performed in excess Cl, the Cl atom sensitivity was found to be nonlinear. Consequently a polynomial function was fitted to the measured chlorine atom intensities obtained during these calibrations. These calibrations were performed at the same temperatures and pressures as the experiments themselves although no temperature dependence of the Cl atom signals was observed.

Chlorine Atom Wall Loss. Chlorine atoms were added to the flow both through a fixed port and via a moveable inlet during the course of the experiments so it was necessary to take into consideration chlorine atom wall losses. It was also necessary to determine the magnitude of these wall losses to calculate the axial and radial diffusion corrections described below. Wall loss measurements were conducted under the same experimental conditions of flow velocities, temperatures, and pressures as the main Cl + HO_2 experiments, although no HO_2 was added to the flows. In these experiments, Cl atoms were generated in the moveable inlet of the flow system via the microwave discharge of a similarly dilute mixture of Cl_2 in He as used for the production of Cl atoms during the course of the experiments. The Cl atoms were then added at different points along the flow tube and the fluorescence intensity was recorded

using the same averaging procedures as described earlier. The resultant semilog plots of fluorescence intensity versus reaction time clearly showed that heterogeneous reactions were first order with respect to loss of Cl. A linear least-squares fit to the slope was then used to determine the rate coefficient for Cl atom wall loss at that temperature. The procedure was then repeated at all of the temperatures used. The measured values, after corrections for diffusional loss have been applied, are listed in Table 1.

HCl Detection. HCl produced in channel 1a of the Cl + HO_2 reaction was monitored using a long path infrared absorption technique. A tunable diode laser (TDL) (Laser Components model DH5) mounted in a liquid nitrogen cooled dewar (Laser Photonics model L5736) produced light at approximately 3.4 μm such that it was coincident with the fundamental vibration−rotation band of HCl. The laser temperature, current, and modulation amplitude were set by a TDL controller (Laser Photonics model L5830). The laser used for this study was typically operated at approximately 84 K with currents ranging between 290 and 330 mA to produce an output at 2944.9 cm^{-1}. This wavelength coincided with the R(2) line of $H^{35}Cl$ and was chosen due to it being the maximum of the Boltzmann distribution at room temperature. The infrared output signals were monitored using an indium antimonide detector with a built in preamplifier (Kolmar Technologies model KISDP-1-J1) that was cooled to 77 K prior to use. To avoid the occurrence of potential multiple absorptions, it was necessary to verify that the laser was operating at a single discrete wavelength (single mode). The cw laser output was modulated at 1100 Hz using a mechanical chopper (EG&G model 197) before being separated into its component wavelengths via a 0.5 m focal length monochromator (Acton model SP500). The output of the monochromator was subsequently detected using a second indium antimonide detector (Infrared Associates model HCT-100) before being demodulated at the reference frequency with a lock-in amplifier (Stanford Research Systems model SR810). A digital-to-analogue (D/A) data acquisition card (Keithley model DAS-16G) connected to a PC allowed the lock-in output to be displayed and stored. During the experiments themselves, the laser was frequency modulated by applying a small amplitude modulation to the laser current. Typically, a 1.4 mA amplitude variation was superimposed on the main current at a frequency of 12.5 kHz. The D/A card was used to scan the laser current across the selected spectral range at a combined resolution for the D/A card and laser controller of 0.0244 mA bit^{-1}. The tuning rate of the laser was 0.068 cm^{-1} mA^{-1}, which gave a spectral step size of 1.7×10^{-3} cm^{-1} bit^{-1}. The laser beam was passed into a Herriott cell[15,16] that was coaxial with the gas flow and downstream of the resonance fluorescence cell. This cell comprised two convergent, spherical gold-coated mirrors 7.6 cm in diameter with a focal length of 45.7 cm. The mirrors were located at a separation of 84.6 cm, which gave rise to a path length of 35.5 m for the 42 passes between the mirrors. Upon exiting the Herriott cell, the attenuated laser beam was collected by the detector−preamplifier and subsequently demodulated at the first harmonic frequency, 2f at 25 kHz by a lock-in amplifier (Stanford Research Systems model SR830). The resultant second derivative absorption signal was then processed by the D/A card before being displayed and stored on a PC. An example of a HCl signal obtained during the course of the experiments is shown in Figure 1. The amplitude of the central positive peak was used as a measure of the HCl concentration.

HCl Calibration. To accurately determine HCl product concentrations, it was important to calibrate the HCl detection

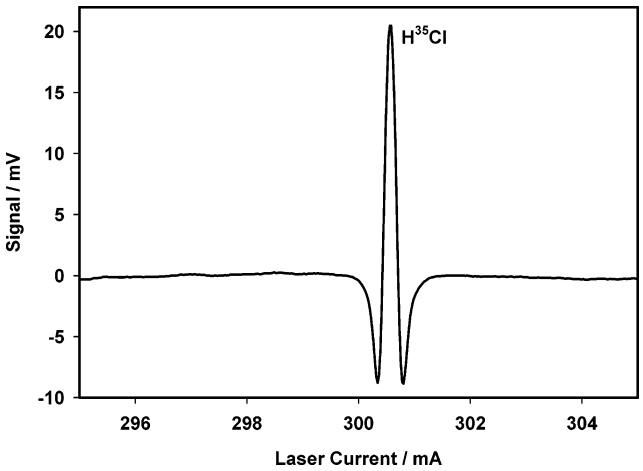

Figure 1. HCl absorption signal of the R(2) line at 2944.91 cm^{-1}. The amplitude of the positive peak is taken as a measure of the signal strength.

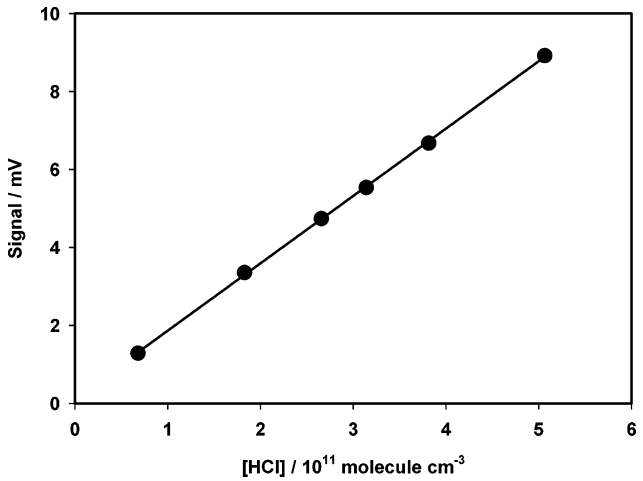

Figure 2. Calibration plot of HCl signal versus [HCl].

sensitivity for each experiment undertaken, especially as the sensitivity was known to be dependent upon the laser operating conditions, the path length, and the optical alignment which could vary from experiment to experiment. The HCl detection sensitivity was determined by flowing a known concentration of HCl through the Herriott cell under similar conditions of pressure and temperature to those used during the experiments. A mixture of a known composition of HCl in He stored in a 5 L Pyrex flask was flowed into the cell upstream of the main reactor using a stainless steel flow meter, the flow being controlled by a Teflon needle valve. During the calibration experiment, the flow meter was initially set by adjusting the needle valve to obtain the required throughput and then the flow meter was bypassed to prevent any HCl losses on its metal interior. All flow lines downstream of this point were constructed from either Pyrex or Teflon to minimize any further heterogeneous loss of HCl. The flow rates were recorded before and after the calibration to measure the average flow rate. The needle valve was then adjusted and the procedure repeated to obtain several measurements of the HCl signal at different known flow rates. A subsequent plot of the HCl concentration determined from the flow against the absorption signal yielded a straight line with the sensitivity, S_{HCl}, as the gradient. An example of a calibration plot is given in Figure 2. The signal was seen to be linear up to [HCl] $\approx 1 \times 10^{12}$ molecule cm^{-3} and S_{HCl} was found to range between 2×10^{-11} and 1×10^{-10} mV cm^3 $molecule^{-1}$. At the minimum sensitivity and at

TABLE 2: Measured Values for k_{1a}[a]

T/K	no. of measurements	$[Cl]/10^{12}$ molecule cm^{-3}	$k_{1a}/10^{-11}$ cm^3 molecule^{-1} s^{-1}
336	15	0.3−2.1	3.6 ± 0.2[b,c]
316	17	0.4−2.2	3.7 ± 0.1
296	16	0.5−2.7	3.6 ± 0.1
276	16	0.6−3.3	3.8 ± 0.1
256	15	0.6−3.3	4.1 ± 0.2
236	14	0.3−2.0	4.7 ± 0.1
226	14	0.3−1.4	5.0 ± 0.1

[a] Corrected for axial and radial diffusion. [b] Errors are cited at the level of a single standard deviation. [c] From plots of k_{1a}[Cl] versus [Cl].

a signal-to-noise of unity, a detection limit of 1×10^9 molecule cm^{-3} could be obtained. In a previous study,[13] the HCl calibrations were checked for possible losses through simultaneous absorption measurements of CH_4 and HCl. These two methods showed no significant discrepancies in the measured HCl concentrations using a similar experimental setup to the current study. Furthermore, experiments in which flows of HCl were passed through the moveable inlet into the main reactor showed no change in the observed HCl absorption while varying the position of the inlet at all temperatures under investigation. As such, no additional checks on the heterogeneous loss of HCl were thought to be necessary.

Calibrations. The mass flow controllers and meters used during the course of the experiments were calibrated for the particular gas mixture to be flowed using a pressure drop/rise at constant volume method. Factory calibrated capacitance manometers were used to calibrate the pressure gauges on the system. The thermocouples used to monitor the cell temperature were calibrated at 273 and 195 K using ice/water and CO_2(s)/ethanol mixtures, respectively. The internal temperature of the flow tube was measured at several positions using a thermocouple probe in place of the usual moveable inlet. At room temperature (296 K) and above, the probe temperature was within 0.1 K of the jacket thermocouple temperatures. At low temperatures the probe temperature and jacket thermocouple temperatures were within 1 K, the probe thermocouple reading the lower of the two. The reported temperatures are those measured using the probe thermocouple.

Corrections. The observed pseudo-first-order rate coefficients were corrected for axial and radial diffusion. The diffusion coefficients for atomic chlorine in He, OH in He, and HO_2 in He were given by $0.0237 \times T^{1.75}$, $0.1447 \times T^{1.5}$, and $0.0332 \times T^{1.71}$ Torr cm^2 s^{-1}, respectively.[17] These gave rise to corrections to the rate coefficients of between 4.1% and 9.4%. No corrections were made for the viscous pressure drop between the reaction zone and the pressure measurement port because earlier observations using the present reactor showed that the corrections were less than 0.5%.

Reagents. High-purity chemicals were used to minimize the introduction of impurities into the flow. Research grade He (99.9999%) was further purified prior to use by flowing through a molecular sieve (Linde 3A) trap held at 77 K. Furthermore, research grade O_2 (99.999%), research grade Cl_2 (99.999%), research grade H_2 (99.9999%), ULSI grade HCl (99.999%), CP grade NO (99%) which was further purified prior to use by flowing through a molecular sieve (Linde 3A) trap held at 195 K, 0.5% and 1% mixtures of F_2 in He, H_2O_2 (90%) which was further purified by pumping prior to use, and NO_2 which was prepared from NO by adding excess O_2 were all used during the course of the experiments.

Kinetic Results

Excess Cl. Cl atom concentrations used were in the range of 3×10^{11} to 3×10^{12} molecule cm^{-3} with initial HO_2 concentrations ranging from 1×10^{10} to 5×10^{10} molecule cm^{-3}. Initial stoichiometric ratios ranged from 6 to 300. O_2 concentrations were between 6×10^{15} and 8×10^{15} molecule cm^{-3}. Measurements were made at temperatures ranging from 226 to 336 K and at an approximate total pressure of 1 Torr of helium.

Data Analysis. Under the conditions described above, the loss of HO_2 radicals was well described by a pseudo-first-order decay profile. When Cl was added to the system, not only did we observe the loss of HO_2, but we also observed the production of OH simultaneously due to the conversion of HO_2 to OH via reaction 1b. After integration of the relevant kinetic equations, it can be written that

$$[HO_2] + [OH] = [HO_2]_0(\exp[-k_1[Cl]t] + k_{1b}/k_1 - (k_{1b}/k_1)\exp[-k_1[Cl]t]) \quad (13)$$

For small values of t, the expansion of $e^x = 1 + x$. Consequently, we can simplify this expression to give

$$[HO_2] + [OH] = [HO_2]_0(1 - k_{1a}[Cl]t) \quad (14)$$

As $\ln(1 - k_{1a}[Cl]t) \approx -k_{1a}[Cl]t$ for $k_{1a}[Cl]t < 1$, it can be written that

$$\ln([HO_2] + [OH]) = \ln[HO_2]_0 - k_{1a}[Cl]t \quad (15)$$

Furthermore, as the OH resonance fluorescence signal, I_{OH}, varied linearly with [OH], i.e., $[OH] = S_{OH}I_{OH}$, and HO_2 was detected as OH and since [Cl] was in excess, it could be written that

$$\ln[I_{HO_2} + I_{OH}] = -k_{1a}'t + \ln[I_{(HO_2)_0}] \quad (16)$$

where $k_{1a}' = k_{1a}[Cl]$. Values of k_{1a}' were determined from the slopes of $\ln(I_{HO_2} + I_{OH})$ against reaction length (l) plots by linear least-squares analysis. Under plug flow conditions, the reaction time was subsequently calculated by the relationship $t = l/v$, where v represents the flow velocity. Typical reaction lengths used varied from 5 to 26 cm giving rise to reaction times of between 3 and 18 ms. A summary of the measured rate coefficients is given in Table 2 and the data obtained at the two extremes of measurement, 336 and 226 K, are presented in Figure 3.

An Arrhenius plot of the data is shown in Figure 4 as ◆ and yields the following expression

$$k_{1a} = (1.6 \pm 0.2) \times 10^{-11}\exp[(249 \pm 34)/T]\ \text{cm}^3\ \text{molecule}^{-1}\ \text{s}^{-1} \quad (17)$$

for $226 \le T \le 336$ K. The measurement errors are obtained from an unweighted linear least-squares analysis and are cited at the level of a single standard deviation.

Excess HO_2. Concentrations of HO_2 were in the range of 4×10^{11} to 4×10^{12} molecule cm^{-3} with initial Cl atom concentrations ranging from 2×10^{10} to 5×10^{10} molecule cm^{-3}. Initial stoichiometric ratios ranged from 6 to 150. H_2O_2 concentrations were between 8×10^{12} and 1.1×10^{13} molecule cm^{-3}. Measurements were made at temperatures ranging from 246 to 296 K and at an approximate total pressure of 1 Torr of helium.

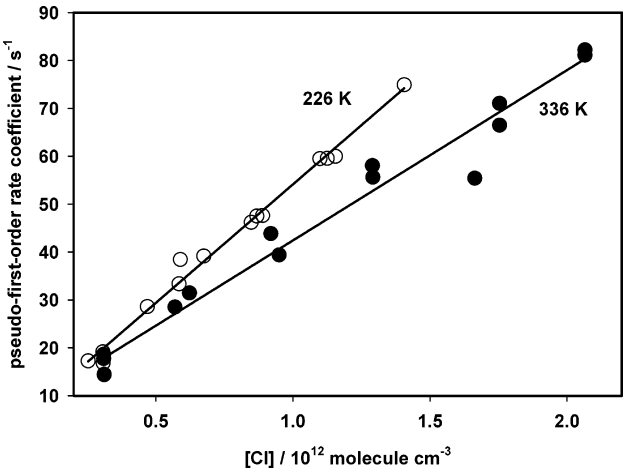

Figure 3. Plots of pseudo-first-order rate coefficient, k_{1a}[Cl] versus [Cl]. All of the data have been corrected for axial and radial diffusion and for HO_2 conversion losses. Lines are linear least-squares fits to the data. Temperatures are given alongside each plot.

TABLE 3: Measured Values for k_1[a]

T/K	no. of measurements	$[HO_2]/10^{12}$ molecule cm^{-3}	$k_1/10^{-11}$ cm^3 molecule^{-1} s^{-1}
296	26	0.4−4.1	4.3 ± 0.1[b,c]
276	10	0.4−3.8	4.4 ± 0.3
256	14	0.4−2.4	4.6 ± 0.2
246	15	0.4−2.3	4.6 ± 0.2

[a] Corrected for axial and radial diffusion. [b] Errors are cited at the level of a single standard deviation. [c] From plots of $k_1[HO_2]$ versus $[HO_2]$.

Data Analysis. Under the conditions described above, the loss of Cl atoms was well described by a pseudo-first-order decay profile. When HO_2 was added to the system, the loss of Cl could be written as

$$-\mathrm{d[Cl]}/\mathrm{d}t = k_1[HO_2][Cl] + k_{L,Cl}[Cl] \quad (18)$$

Here $k_{L,Cl}$ represents the pseudo-first-order loss of Cl atoms in the absence of HO_2. This was thought to be due to heterogeneous reactions and also some secondary gas-phase reactions may have contributed. As the Cl resonance fluorescence signal, I_{Cl}, varied linearly with [Cl] at the low concentrations used in these experiments, i.e., $[Cl] = S_{Cl}I_{Cl}$, and $[HO_2]$ was in excess, it could be written that

$$-\mathrm{d}\ln[I_{Cl}]/\mathrm{d}t = k_1' + k_{L,Cl} \quad (19)$$

where $k_1' = k_1[HO_2]$. Values of $k_1' + k_{L,Cl}$ were determined from the slopes of $\ln(I_{Cl})$ against reaction length (l) plots by linear least-squares analysis. Under plug flow conditions, the reaction time was subsequently calculated by the relationship $t = l/v$, where v represents the flow velocity. Typical reaction lengths used varied from 5 to 34 cm giving rise to reaction times of between 3 and 22 ms. A summary of the measured rate coefficients is given in Table 3 and the data obtained at the two extremes of measurement, 296 and 246 K, are presented in Figure 5.

An Arrhenius plot of the data is shown in Figure 4 as ▼ and yields the following expression

$$k_1 = (2.8 \pm 0.1) \times 10^{-11} \exp[(123 \pm 15)/T] \text{ cm}^3 \text{ molecule}^{-1} \text{ s}^{-1} \quad (20)$$

for $246 \le T \le 296$ K. The measurement errors are obtained from an unweighted linear least-squares analysis and are cited at the level of a single standard deviation. Experiments were limited to temperatures greater than 246 K due to the difficulty of producing HO_2 in excess. As this expression exhibits only a weakly negative temperature dependence, we report a temperature-independent value for $k_1 = (4.5 \pm 0.4) \times 10^{-11}$ cm^3 molecule^{-1} s^{-1}. Furthermore, as $k_1 = (k_{1a} + k_{1b})$ it is evident that we can derive an Arrhenius expression for k_{1b} by a simple subtraction of the experimentally determined values of k_{1a} from the temperature-independent value for k_1 at the temperatures where the experimental values coincide (256, 276, and 296 K). This results in

$$k_{1b} = (7.7 \pm 0.8) \times 10^{-11} \exp[(-708 \pm 29)/T] \text{ cm}^3 \text{ molecule}^{-1} \text{ s}^{-1} \quad (21)$$

This expression is valid over the range $256 \le T \le 296$ K and is plotted in Figure 4 as ◇ alongside the previously determined values for k_{1b}.

Product Results

OH Yields. To obtain the OH product yield from reaction 1b it was necessary to measure the amount of OH produced for a given amount of HO_2 reacted. We can write the rate of HO_2 loss and the rate of OH production as

$$-\mathrm{d[HO_2]}/\mathrm{d}t = k_1[HO_2][Cl] \quad (22)$$

$$\mathrm{d[OH]}/\mathrm{d}t = k_{1b}[HO_2][Cl] \quad (23)$$

Integrating and combining these equations from time zero to time t gives

$$[OH] = k_{1b}/k_1[HO_2]_0(1 - \exp[-k_1[Cl]t]) \quad (24)$$

As $k_1[Cl]t$ becomes large, it can be written that

$$[OH]_\infty/[HO_2]_0 = k_{1b}/k_1 \quad (25)$$

Furthermore, as $[OH] = S_{OH}I_{(OH)}$ and $[HO_2] = S_{OH}I_{(HO_2)}$, we can write

$$I_{(OH)\infty}/I_{(HO_2)_0} = k_{1b}/k_1 \quad (26)$$

$[OH]_\infty$ represents the amount of OH produced for a consumption of HO_2 approaching 100%. $I_{(OH)\infty}$ represents the corresponding OH resonance fluorescence signal. $[HO_2]_0$ and $I_{(HO_2)_0}$ are the initial HO_2 concentration and the initial HO_2 (detected as OH) resonance fluorescence signal, respectively. The OH product measurements were performed under the conditions of Cl in excess over HO_2 with Cl atom concentrations ranging from 9.0×10^{12} to 1.3×10^{13} molecule cm^{-3}. HO_2 was generated via reaction 3 in all of the product measurements reported in this study. HO_2 concentrations were varied by changing the flow rate of H_2 into the HO_2 pre-reactor and ranged from 1.0×10^{10} to 1.5×10^{11} molecule cm^{-3}. A 4% mixture of H_2 in He was flowed into the system in the range of 0.15−2.2 sccm. During the product experiments, an initial measurement of $I_{(HO_2)_0}$ was made with NO flowing but in the absence of Cl. Subsequently, Cl was added to the system through the moveable inlet at a reaction length of approximately 34 cm, which corresponded to reaction times ranging from 16 to 22 ms. The NO flow was turned off and the signal due to product OH, $I_{(OH)\infty}$, was recorded. The experiment was then repeated at several H_2 flows

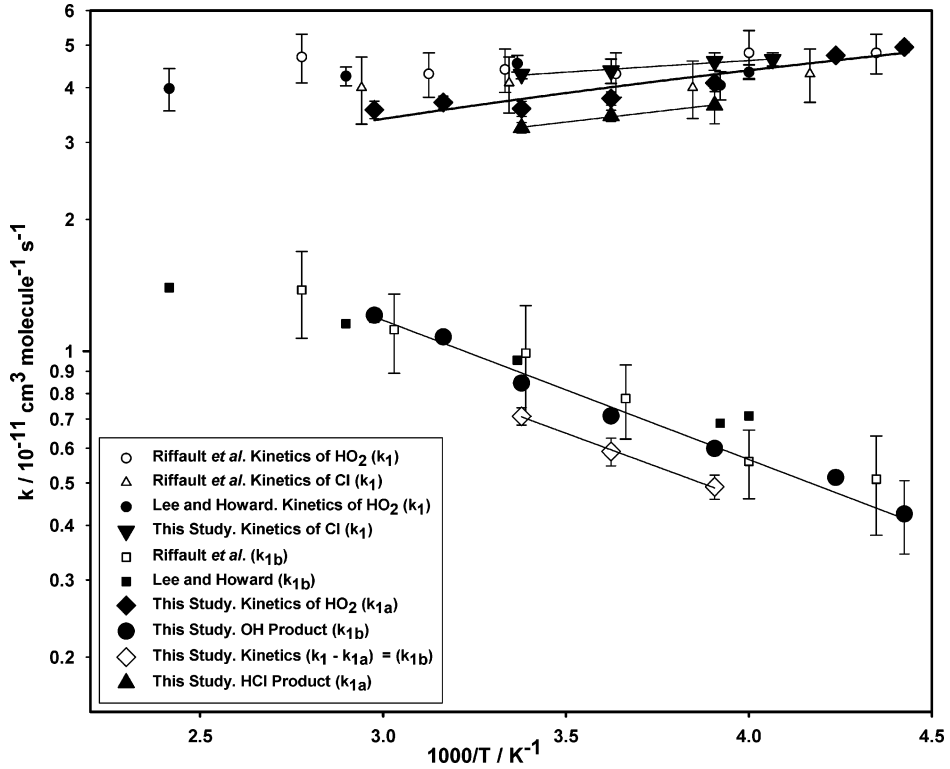

Figure 4. Arrhenius plot of the present results compared to earlier studies. Lines are the unweighted linear least-squares fits to the present data. The error bars on our data represent a single standard deviation.

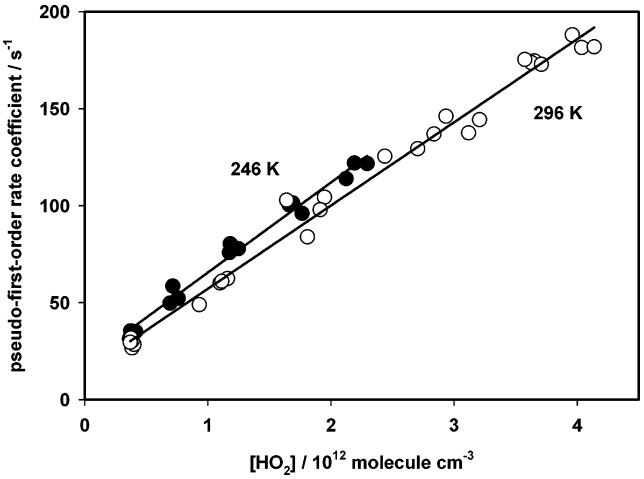

Figure 5. Plots of pseudo-first-order rate coefficient, $k_1[HO_2]$ versus $[HO_2]$. All of the data have been corrected for axial and radial diffusion. Lines are linear least-squares fits of the data. Temperatures are given alongside each plot.

to vary $[HO_2]_0$. A plot of $I_{(OH)\infty}$ versus $I_{(HO_2)_0}$ gave rise to a straight line from which a linear least-squares analysis yielded the product branching ratio from the gradient. A plot of $I_{(OH)\infty}$ versus $I_{(HO_2)_0}$ at the two extremes of temperature measurement, 226 and 336 K, is shown in Figure 6.

The measured values for the branching ratio k_{1b}/k_1 are presented in Table 4 and have been corrected for losses incurred during the conversion of HO_2 to OH via reaction 5. These values are plotted in Figure 7 alongside the previously determined values for the OH product yield.

HCl Yields. To measure the branching ratio, k_{1a}/k_1, it was necessary to measure the HCl product yield for a given amount of HO_2 reacted. The rates of loss of HO_2 and formation of HCl are shown below.

$$-\mathrm{d}[HO_2]/\mathrm{d}t = k_1[HO_2][Cl] \quad (22)$$

$$\mathrm{d}[HCl]/\mathrm{d}t = k_{1a}[HO_2][Cl] \quad (27)$$

In a manner analogous to that for the OH product yields, at large $k_1[Cl]t$ it can be written that

$$[HCl]_\infty/[HO_2]_0 = k_{1a}/k_1 \quad (28)$$

As before, $[HCl]_\infty$ represents the amount of HCl produced for a consumption of HO_2 approaching 100% and $[HO_2]_0$ represents the initial HO_2 concentration. Initial reactant concentrations were identical with those used in the OH product experiments. Unlike the OH product yield measurements, however, which used the same technique for both OH and HO_2 detection (as HO_2 was converted to OH), it was necessary to calculate actual concentrations for a quantitative measurement of the HCl product yield. As such, calibrations of the OH intensity and the HCl intensity, as described in earlier sections of this paper, were performed alongside the experiments themselves. During these experiments, an initial measurement of $I_{(HO_2)_0}$ was made with NO on but in the absence of Cl. Subsequently, Cl was added to the system through the moveable inlet at a reaction length of approximately 34 cm, which corresponded to reaction times ranging from 110 to 114 ms at the midpoint of the Herriott cell where HCl was monitored. The NO flow was turned off and the absorption due to product HCl and background HCl, $I_{(HCl)\infty} + I_{(HCl),bkd}$, was recorded. The H_2 microwave discharge was then switched off, and the absorption due to background HCl alone, $I_{(HCl),bkd}$, was recorded. Background HCl was predominantly produced through the reaction of Cl with hydrocarbon wax coating the inside surfaces of the reactor. The relative sizes of these absorptions, which varied between $5 \leq I_{(HCl)\infty}/I_{(HCl),bkd} \leq 30$ were dependent upon $[HO_2]_0$, with small values of $[HO_2]_0$ leading to small values for the above ratio. The experiment was then repeated at several H_2 flows to vary $[HO_2]_0$. Measurements of the HO_2 sensitivity,

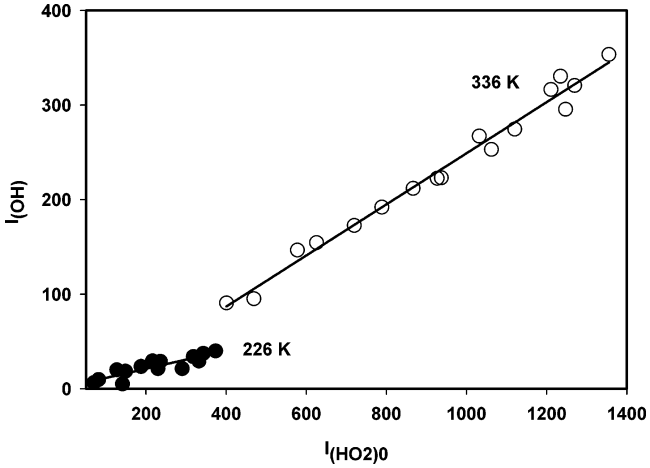

Figure 6. OH signal versus initial HO_2 signal. HO_2 intensities have been corrected for $HO_2 \rightarrow$ OH conversion losses. Lines are the unweighted linear least-squares fits to the present data. Temperatures are given alongside each plot.

TABLE 4: OH Yields from Product Measurements[a]

T/K	no. of measurements	OH yield/%
336	17	27.0 ± 1.0[b,c]
316	15	24.1 ± 0.5
296	20	18.9 ± 0.3
276	13	15.9 ± 0.2
256	22	13.4 ± 0.4
236	27	11.5 ± 0.3
226	14	9.5 ± 1.6

[a] Corrected for $HO_2 \rightarrow$ OH conversion losses. [b] Errors are cited at the level of a single standard deviation. [c] From plots of $I_{(OH)\infty}$ versus $I_{(HO_2)0}$.

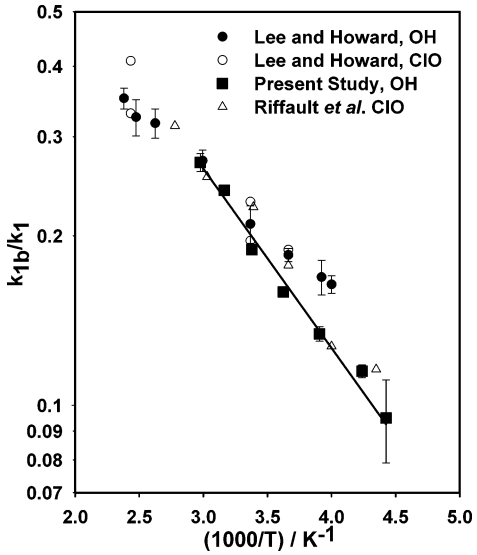

Figure 7. Relative Arrhenius plot of the present results for k_{1b}/k_1 compared to earlier studies. The line is the unweighted linear least-squares fit to the present data. The error bars on our data represent a single standard deviation.

$S_{HO2} \equiv S_{OH}$, and the HCl sensitivity, S_{HCl}, were then taken to convert the measured intensities to absolute concentrations. A plot of $[HCl]_\infty$ versus $[HO_2]_0$ then gave rise to a straight line from which a linear least-squares analysis yielded the product branching ratio k_{1a}/k_1 from the gradient of the slope. A plot of

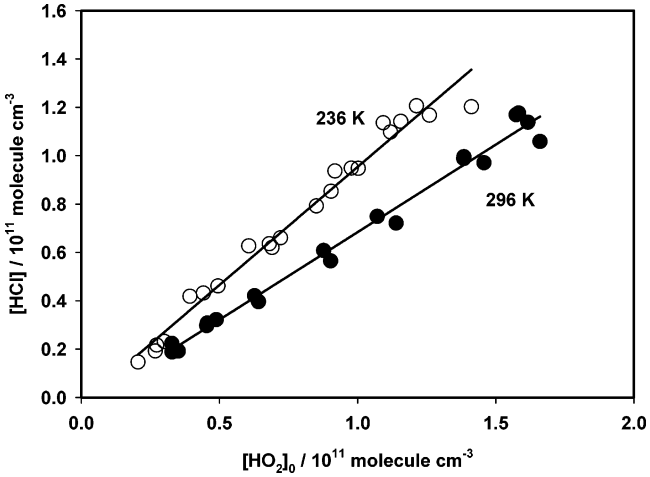

Figure 8. [HCl] yield versus $[HO_2]_0$. HO_2 concentrations have been corrected for $HO_2 \rightarrow$ OH conversion losses and for HO_2 wall losses. Lines are the unweighted linear least-squares fits to the present data. Temperatures are given alongside each plot.

TABLE 5: HCl Yields from Product Measurements[a]

T/K	no. of measurements	HCl yield/%
296	20	72.4 ± 2.0[b,c]
276	13	77.1 ± 2.3
256	22	81.5 ± 2.1
236	27	97.7 ± 3.2

[a] Corrected for $HO_2 \rightarrow$ OH conversion losses and for HO_2 wall losses. [b] Errors are cited at the level of a single standard deviation. [c] From plots of $[HCl]_\infty$ versus $[HO_2]_0$.

$[HCl]_\infty$ versus $[HO_2]_0$ at the two extremes of temperature measurement, 236 and 296 K, is shown in Figure 8.

The measured values for the branching ratio k_{1a}/k_1 are presented in Table 5 and have been corrected for HO_2 wall losses in addition to the losses incurred during the conversion of HO_2 to OH via reaction 5. No HCl wall losses were observed at any of the temperatures used in this study. These values are also plotted in Figure 9. It should be noted that the previously determined yields for k_{1a}/k_1 are simply subtractions of the previously determined values for k_{1b}/k_1, i.e. $(1 - k_{1b}/k_1)$.

Discussion

Numerical Modeling and Secondary Chemistry. Computer models were used to check for losses incurred during the NO + HO_2 reaction for the conversion of HO_2 to OH and also to check for possible interference from secondary reactions in the kinetic and product studies. The simulations were carried out using the CHEMRXN program, which has been validated versus a standard differential integrator and a stochastic algorithm.[18] The rate coefficients used in the models were taken from the NASA-JPL Chemical Kinetics Data Evaluation,[11] the IUPAC Gas Kinetics Data Evaluation,[12] and the NIST Chemical Kinetics Database.[19]

Models were used to test for losses of OH and HO_2 during the HO_2 + NO reaction. Concentrations of initial HO_2 were in the range 1×10^{10} to 6×10^{12} molecules cm^{-3}; this covered the concentration range used in the experiments. NO was added at a concentration of 2×10^{14} molecules cm^{-3} and the model was run for 3 ms to simulate the actual laboratory runs. The [OH] calculated at 3 ms was plotted versus $[HO_2]_0$; this plot was then parametrized and used to correct the experimental data. The size of the corrections depended on $[HO_2]_0$ and varied from

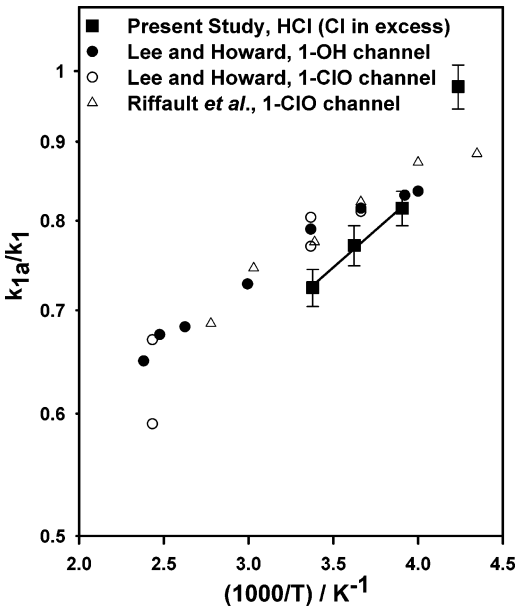

Figure 9. Relative Arrhenius plot of the present results for k_{1a}/k_1 compared to earlier studies. All of the data from earlier studies are subtractions of the k_{1b}/k_1 ratio. The line is the unweighted linear least-squares fit to the present data. The error bars on our data represent a single standard deviation.

2% at the lowest concentrations to about 30% at the highest values; the average correction was about 8%.

We modeled the kinetic experiments using both excess Cl atoms and excess HO_2 at 298 and 236 K. The concentrations used in the models were similar to the experimental values. In the case of excess Cl atoms, initial [Cl] ranged from 2.0×10^{11} to 3.0×10^{12} atoms cm^{-3} with initial [HO_2] between 1.0×10^{10} and 5.0×10^{10} molecules cm^{-3}. The model output consisted of HO_2 and OH concentrations versus time. These were treated in the same way as the experimental data by plotting ln{[HO_2] + [OH]} versus time. Least-squares fits to the data were used to obtain initial slopes, from which values for k_{1a}(out) could be calculated. The change in k_{1a} induced by secondary reactions was then obtained using the following relation: del % = $\{[k_{1a}(\text{out})/k_{1a}(\text{in})] - 1\} \times 100$. The parameter k_{1a}(in) is the rate coefficient used in the model. The results at 298 K are plotted in Figure 10. The effects of secondary chemistry are seen to be less than 8% over the range of concentrations used in the study. At 236 K the effects were less than 6%. No corrections for this have been made since it is well within the experimental error.

For excess HO_2, initial [HO_2] was varied from 4.0×10^{11} to 4.0×10^{12} molecules cm^{-3}; initial [Cl] ranged from 1.0×10^{10} to 5.0×10^{10} atoms cm^{-3}. In this case the model k_1(out) was obtained from the slope of ln[Cl] versus time plots. The change in k_1 due to secondary chemistry was calculated as above and plotted in Figure 10 for runs at 298 K. The effect of secondary chemistry is less than about 10% at low [HO_2] and less than 3% at higher concentrations. At 236 K the effect was less than 6%. No corrections were made.

Model calculations were also used to evaluate possible interference from secondary reactions on the product yield experiments at 298 and 236 K. As in the kinetic simulations, concentrations, reaction times, and data analyses used in the models were similar to those used in the experiments. In the case of OH product, the model yield was obtained from OH concentrations with excess Cl present and [HO_2] without Cl in the system. No corrections for wall losses of OH or HO_2 were made because these losses were similar for both radicals and tended to cancel out. However, HO_2 concentrations were corrected for losses incurred during the conversion to OH with excess NO. The model yield was then calculated from the ratio of [OH] to [HO_2]. The effect of secondary chemistry on the OH yield at 236 K is plotted in Figure 11. The effect ranges from 2.5% to 8% and no corrections were made to the observed OH yields.

In the case of HCl product, the model was run to long reaction times simulating detection in the Herriott cell downstream of the main reaction zone. The model yield was then obtained from the calculated [HCl] at long reaction times and [HO_2] at the resonance cell. No corrections were made to [HCl] but the [HO_2] was corrected as above for losses during the conversion to OH by excess NO and for wall losses. The results at 236 K are presented in Figure 11 although calculations were also performed at 298 K. The effects of secondary chemistry predicted by the model range from 1.5% to 6.5% over the range of concentrations and temperatures used in the experiments and no corrections were made to the observed HCl yields.

Comparison with Earlier Kinetic Work. The previously determined values for the total rate coefficient, k_1, of the Cl + HO_2 reaction are summarized in Table 6. Leu and Demore,[1] Poulet et al.,[2] and Burrows et al.[3] used mass spectrometric detection[1,2] or laser magnetic resonance detection[3] of HO_2 generated by the reaction

$$\text{Cl} + \text{H}_2\text{O}_2 \rightarrow \text{HCl} + \text{HO}_2 \qquad (29)$$

$$k_{29}(298\text{K}) = 4.1 \times 10^{-13}\ \text{cm}^3\,\text{molecule}^{-1}\,\text{s}^{-1}\ \text{(ref 11)}$$

in low-pressure discharge-flow systems. They measured the rate of loss of HO_2 through reaction 1 relative to reaction 29. Cox[4] measured the rate of loss of HO_2 produced in reaction 3 relative to reaction 30

$$\text{Cl} + \text{H}_2 \rightarrow \text{HCl} + \text{H} \qquad (30)$$

$$k_{30}(298\text{K}) = 1.6 \times 10^{-14}\ \text{cm}^3\,\text{molecule}^{-1}\,\text{s}^{-1}\ \text{(ref 11)}$$

It can be seen that although there is scatter in the measurements, the quoted errors in the measurements means that there is reasonable agreement between the values for k_1 derived by previously determined indirect studies and the value obtained here. It should be noted that these indirectly determined numbers have been updated to reflect the currently recommended data[11] for reactions 29 and 30. Cox and Derwent[5] and Cattell and Cox[6] used the flash photolysis technique coupled with UV absorption of mixtures of $Cl_2-H_2-O_2$ and $Cl_2-H_2-O_2-N_2$, respectively. The UV absorptions of Cl_2[5] or of both HO_2 and ClO[6] were monitored and the corresponding concentrations were fit to a complex mechanism where the rate coefficient values for reaction 1 or reactions 1a and 1b separately were allowed to vary until a best fit was obtained. The values for k_1 obtained by Cattell and Cox[6] are in good agreement with this study although the earlier work by Cox and Derwent[5] is certainly outside the range of our error limits. Lee and Howard,[7] Dobis and Benson,[8] and Riffault et al.[9] all undertook direct measurements of k_1. It can be seen that all three studies are in excellent agreement with each other and with the work presented here, especially as these studies were performed using a range of methods and detection techniques. The study by Lee and Howard[7] operated in the regime of [Cl] $\gg$ [HO_2] monitoring the decay of HO_2. They determined a weakly negative temperature dependence for $k_1 = (3.87 \pm 0.54) \times 10^{-11} \exp[(25 \pm 42)/T]$ cm^3 molecule^{-1} s^{-1}. Riffault et al.[9] measured k_1 under

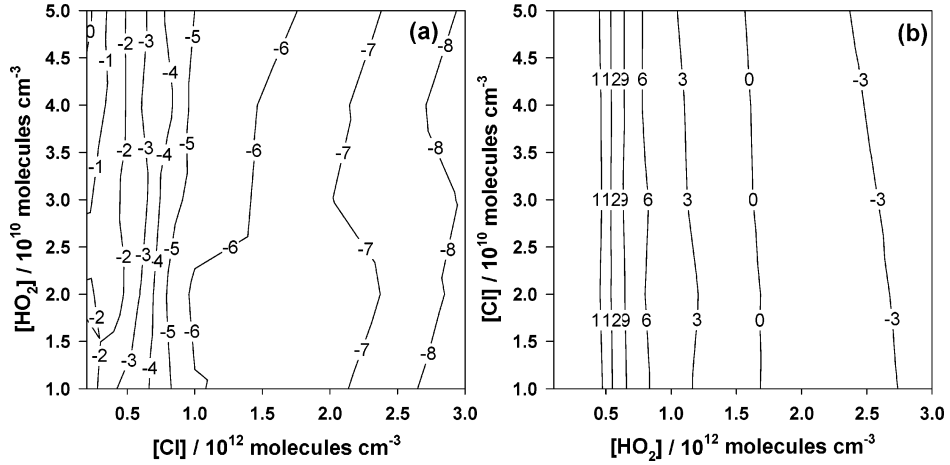

Figure 10. (a) Calculated percentage differences in modeled k_{1a}(out/in) at 298 K with excess Cl. (b) Calculated percentage differences in modeled k_1(out/in) at 298 K with excess HO_2. Percentages reflect the differences between output/input pseudo-first-order rate coefficients.

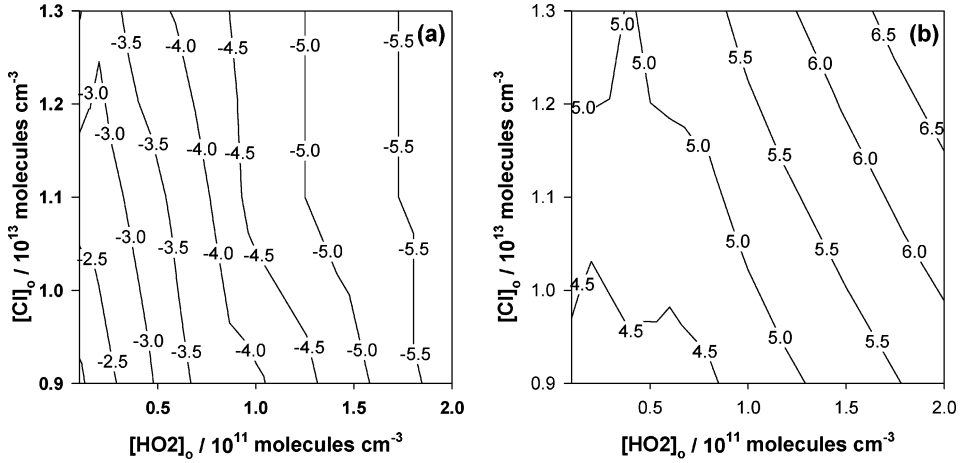

Figure 11. (a) Calculated percentage differences between output and input modeled OH yield at 236 K. (b) Calculated percentage differences between output and input modeled HCl yield at 236 K. Calculations performed in excess Cl.

TABLE 6: Summary of Data for the Rate Coefficient for the Reaction Cl + HO_2 → Products, k_1

T/K	*P*/Torr	$k_1/10^{-11}$ cm^3 molecule^{-1} s^{-1}	technique	method[b]	reference
295	1−2	$1.9^{+2.9}_{-1.2}$ [a]	DF-MS	RR	Leu and Demore[1]
298	0.24−0.36	6.8 ± 2.5[a]	DF-MS	RR	Poulet et al.[2]
298	∼2	4.4 ± 1.5[a]	DF-LMR	RR	Burrows et al.[3]
274−338	760	6.0 ± 3.0[a]	FP-UV	RR	Cox[4]
306	760	2.5 ± 1.0[a]	FP-UV	CM	Cox and Derwent[5]
308	50−760	$4.4^{+4.4}_{-2.2}$ [a]	FP-UV	CM	Cattell and Cox[6]
250−414	0.9−1.5	4.2 ± 0.7[a]	DF-LMR	ABS	Lee and Howard[7]
243−368	∼0.001	4.45 ± 0.06[a]	VLPR-MS	ABS	Dobis and Benson[8]
230−360	∼1	4.4 ± 0.6[a]	DF-MS	ABS	Riffault et al.[9]
256−296	∼1	4.5 ± 0.4[b]	DF−RF	ABS	This Work
250−420		4.2 ± 0.7[a]		EVAL	Sander et al.[11]
230−420		4.3		EVAL	Atkinson et al.[12]

[a] Errors are cited at the level quoted by these authors. [b] Errors are cited at the level of a single standard deviation. RR = relative rate, CM = complex mechanism, ABS = absolute method, and EVAL = evaluation.

the conditions of both [Cl] ≫ [HO_2] and [HO_2] ≫ [Cl] and also calculated a weakly negative temperature dependence for $k_1 = (3.8 \pm 0.6) \times 10^{-11} \exp[(40 \pm 90)/T]$ cm^3 molecule^{-1} s^{-1}. Considering the experimental uncertainties, both sets of authors quote the temperature-independent values for k_1 listed in Table 6. In a manner similar to both Lee and Howard[7] and Riffault et al.[8] we obtain a weakly negative temperature dependence for $k_1 = (2.8 \pm 0.1) \times 10^{-11} \exp[(123 \pm 15)/T]$ under the conditions of [HO_2] ≫ [Cl] and therefore quote a temperature-independent value of $k_1 = (4.5 \pm 0.4) \times 10^{-11}$ cm^3 molecule^{-1} s^{-1} over the range 246−296 K. This value agrees well with current evaluations[11,12] of the available data for k_1.

Table 7 reports all of the previously determined data for the two individual reaction channels 1a and 1b. Under the conditions of [Cl] ≫ [HO_2] we observed the decay of HO_2 radicals via conversion to OH initially. Consequently, we also monitored the formation of product OH radicals simultaneously and an analysis of the relevant rate expressions 13 to 16 led to the conclusion that we only measured k_{1a} by this method. It should be noted that although Lee and Howard[7] and Riffault et al.[9]

TABLE 7: Summary of Data for the Rate Coefficients k_{1a} and k_{1b}

T/K	k_{1a}/cm^3 molecule^{-1} s^{-1}	k_{1b}/cm^3 molecule^{-1} s^{-1}	reference
298		$<3\times10^{-13}$	Burrows et al.[3]
308		$(9.4^{+9.4}_{-4.7})\times10^{-12}$ [a]	Cattell and Cox[6]
250−414	$1.8\times10^{-11}\exp(170/T)$	$4.1\times10^{-11}\exp(-450/T)$	Lee and Howard[7]
		$(9.1\pm1.3)\times10^{-12}$ ($T=298$ K)[a]	
243−368		$(2.2\pm1.4)\times10^{-12}$[a]	Dobis and Benson[8]
230−360		$8.6\times10^{-11}\exp(-660/T)$	Riffault et al.[9]
		$(9.4\pm1.9)\times10^{-12}$ ($T=298$ K)[a]	
226−336	$1.6\times10^{-11}\exp(249/T)$	$7.7\times10^{-11}\exp(-708/T)$	this work (kinetic)
	$(3.6\pm0.1)\times10^{-11}$ ($T=296$ K)	$(7.1\pm1.7)\times10^{-12}$ ($T=296$ K)[b,c]	
250−420	$1.8\times10^{-11}\exp(170/T)$	$4.1\times10^{-11}\exp(-450/T)$	Sander et al.[10]
	3.2×10^{-11} ($T=298$ K)	9.1×10^{-12} ($T=298$ K)	
230−420		$6.3\times10^{-11}\exp(-570/T)$	Atkinson et al.[11]
	3.4×10^{-11} ($T=298$ K)	9.3×10^{-12} ($T=298$ K)	

[a] Errors are cited at the level quoted by these authors. [b] Errors are cited at the level of a single standard deviation. [c] Room temperature (296 K) values are the actual experimental numbers and are not derived from the fit.

also operated under the conditions of [Cl] ≫ [HO_2], they observed HO_2 loss and OH product formation as separate processes. The solution of the relevant rate equations for their systems produces the result that the total rate coefficient, k_1, was measured by this method. The values for k_1 of Riffault et al.[9] quoted in Table 6 are therefore based on data obtained with both [Cl] ≫ [HO_2] and [HO_2] ≫ [Cl]. To date, the current study represents the only direct measurement of $k_{1a} = (1.6 \pm 0.2) \times 10^{-11}\exp[(249 \pm 34)/T]$ for $226 \le T \le 336$ K although the current NASA panel recommendation[11] provides an estimate of the Arrhenius parameters for this channel based on a knowledge of the Arrhenius parameters for k_1 and k_{1b} provided by Lee and Howard.[7] The agreement between these estimated values and our direct measurement of the same parameters is good although the recommended Ea/R value falls outside our error limits. We determine that $k_{1a}(296\text{K}) = (3.6 \pm 0.1) \times 10^{-11}$ cm^3 molecule^{-1} s^{-1}, which compares reasonably well with the current evaluations[11,12] also listed in Table 7 although both recommend slightly lower values at room temperature.

Previous measurements of the kinetics of channel 1b fall into two categories. The first category of measurements[3,8] conclude that reaction 1b has only a small role in the overall kinetics of reaction 1. Burrows et al.[3] were unable to observe any OH product formation during their experiments, which led them to report an upper limit for $k_{1b}(298\text{K}) < 3\times10^{-13}$ cm^3 molecule^{-1} s^{-1}. Similarly, using a VLPR technique coupled with MS detection, Dobis and Benson[8] measured $k_{1b}(298\text{K}) = (2.2 \pm 1.4) \times 10^{-12}$ cm^3 molecule^{-1} s^{-1} although no temperature dependence could be obtained due to the large scatter in the experimental data.

In contrast, the second category of measurements[6,7,9] conclude that the endothermic channel 1b plays a more significant role in the partitioning of reaction 1. Cattell and Cox[6] obtained $k_{1b}(308\text{K}) = (9.4^{+9.4}_{-4.7}) \times 10^{-12}$ cm^3 molecule^{-1} s^{-1} using a complex fitting procedure of the measured data from their UV photolytic system. Lee and Howard[7] detected both OH and ClO products in separate experiments to measure the branching fraction k_{1b}/k_1. A linear least-squares fit to the data subsequently yielded the relative Arrhenius expression $k_{1b}/k_1 = (1.09 \pm 0.06)\exp[-(478 \pm 17)/T]$. Arrhenius parameters for reaction 1b were inferred by combining the observed branching ratios with their measured values of k_1. Riffault et al.[9] also detected both OH and ClO products but from the initial reactants Cl atoms and H_2O_2. HO_2 radicals were generated through reaction 29 and the changes in concentrations of Cl, ClO, OH, and HO_2 were observed with time. The resultant experimental profiles were fitted by allowing only the variation of two parameters: k_1 and the branching fraction k_{1b}/k_1. The best fit to the data was obtained with $k_1 = (4.0 \pm 0.2) \times 10^{-11}$ cm^3 molecule^{-1} s^{-1} and $k_{1b}/k_1(298\text{K}) = 0.22 \pm 0.01$. The procedure was repeated at a range of temperatures to yield the Arrhenius expression $k_{1b} = (8.6 \pm 3.2)\exp[-(660 \pm 100)/T]$ cm^3 molecule^{-1} s^{-1}. In the current study, we have not directly measured k_{1b} by kinetic methods, but in a manner analogous to that used by Lee and Howard[7] we can infer values for k_{1b} from a subtraction of the respective k_1 and k_{1a} data. An Arrhenius fit to the three data points where values overlap (from k_1 to k_{1a} at 256, 276, and 296 K) gives $k_{1b} = (7.7 \pm 0.8) \times 10^{-11}\exp[-(708 \pm 29)/T]$ cm^3 molecule^{-1} s^{-1} for $256 \le T \le 296$ K and $k_{1b}(296\text{K}) = (7.1 \pm 1.7) \times 10^{-12}$ cm^3 molecule^{-1} s^{-1}. The derived Arrhenius parameters from this study are close to those previously determined by Lee and Howard[7] and by Riffault et al.[9] and show a similar significant positive temperature dependence for k_{1b} although these earlier studies lie outside our error limits. Furthermore, our room-temperature value is in good general agreement with the values of Cattell and Cox,[6] Lee and Howard,[7] and Riffault et al.[9] by giving a much larger significance to reaction 1b compared to the determinations by Burrows et al.[3] and Dobis and Benson.[8]

As a further examination of the Cl + HO_2 chemical system, we also studied the temperature dependence of the product formation channels in experiments separate from those already mentioned above. In these experiments, the concentrations of HCl and OH formed in reactions 1a and 1b respectively were measured as a function of the initial HO_2 concentration over a range of temperatures. The derived relative Arrhenius expressions for the branching ratios k_{1a}/k_1 and k_{1b}/k_1 are

$$k_{1a}/k_1 = (3.4 \pm 0.2) \times 10^{-1}\exp[(222 \pm 17)/T] \quad (256 \le T \le 296\ \text{K}) \quad (31)$$

$$k_{1b}/k_1 = (2.4 \pm 0.3)\exp[-(733 \pm 41)/T] \quad (226 \le T \le 336\ \text{K}) \quad (32)$$

Although data were obtained at 236 K for the ratio k_{1a}/k_1 as shown in Figure 9, these data points have been excluded from the dataset used in the calculation of expression 31. It is apparent that at this temperature there may have been a heterogeneous source of HCl unaccounted for by the normal HCl background subtraction method.

These expressions can be converted to absolute numbers using the temperature-independent value of $k_1 = (4.5 \pm 0.4) \times 10^{-11}$ cm^3 molecule^{-1} s^{-1} determined in this study by kinetic methods. The derived Arrhenius expressions and room temperature rate coefficients are shown in Table 8 and displayed graphically in Figure 4 as ▲ and ● for k_{1a} and k_{1b}, respectively.

TABLE 8: Arrhenius Parameters and Rate Coefficients Derived from Product Data

T/K	k_{1a}/cm^3 molecule^{-1} s^{-1}	k_{1b}/cm^3 molecule^{-1} s^{-1}
256−296	$(1.5 \pm 0.1) \times 10^{-11} \exp[(222 \pm 17)/T]$[a]	
	$(3.2 \pm 0.1) \times 10^{-11}$ ($T = 296$ K)[b]	
226−336		$(10.6 \pm 1.5) \times 10^{-11} \exp[-(733 \pm 41)/T]$
		$(8.5 \pm 0.1) \times 10^{-12}$ ($T = 296$ K)[b]

[a] Errors are cited at the level of a single standard deviation. [b] Room temperature (296 K) values are the actual experimental numbers and are not derived from the fit.

The parameters for k_{1a} and k_{1b} listed in Tables 7 and 8 obtained in this study by independent kinetic and product experiments are in good agreement, especially with respect to the values derived for k_{1a}. This is particularly notable as different experimental techniques were used for the kinetic and product experiments. The kinetic measurements for k_{1a} utilized resonance fluorescence of the loss of HO_2 reagent whereas the product measurements used long path IR absorption for the detection of HCl product. There seems to be a discrepancy, however, between the derived preexponential factors from kinetic and product experiments for k_{1b} although the activation energies compare favorably. This discrepancy translates to values of $k_{1b}(298\text{K}) = 7.2 \times 10^{-11}$ and 9.1×10^{-11} cm^3 molecule^{-1} s^{-1} from the fits for kinetic and product determinations, respectively, a difference of approximately 20%. At 256 K this difference becomes approximately 30% from the fits. This discrepancy, although significant, is still indicative of a greater contribution by channel 1b to the overall loss of HO_2 through reaction 1 than determined by Burrows et al.[3] and Dobis and Benson.[8] The separate datasets from kinetic and product experiments can be combined to derive two final Arrhenius expressions for k_{1a} and k_{1b}:

$$k_{1a} = (1.4 \pm 0.3) \times 10^{-11} \exp[(269 \pm 58)/T] \text{ cm}^3 \text{ molecule}^{-1} \text{ s}^{-1} \quad (33)$$

$$k_{1b} = (12.7 \pm 4.1) \times 10^{-11} \exp[-(801 \pm 94)/T] \text{ cm}^3 \text{ molecule}^{-1} \text{ s}^{-1} \quad (34)$$

These expressions are both reported for the temperature range $226 \le T \le 336$ K.

In addition to the derived kinetic equations, we can also calculate thermochemical parameters due to the reversibility of reaction 1b:

$$\text{Cl} + \text{HO}_2 \rightleftharpoons \text{OH} + \text{ClO} \qquad (1\text{b}, 2\text{a})$$

The enthalpy of reaction, ΔH_r, can be calculated by using the van't Hoff equation, $-RT \ln K_{eq} = \Delta H_r - T\Delta S_r$, and by plotting $\ln(K_{eq})$ against $1/T$. Using $k_{1b} = (12.7 \pm 4.1) \times 10^{-11} \exp[-(801 \pm 94)/T]$ cm^3 molecule^{-1} s^{-1} from this study and $k_{2a} = (7.2 \pm 2.2) \times 10^{-12} \exp[(333 \pm 70)/T]$ cm^3 molecule^{-1} s^{-11} from the study by Wang and Keyser[20] we obtain $\Delta H_r = (2.3 \pm 0.3)$ kcal mol^{-1}. This also yields a value for the reaction entropy ΔS_r of (5.7 ± 2.5) cal mol^{-1} deg^{-1}. Using the known heats of formation for OH, ClO, and Cl of 8.9, 24.3, and 29.0 kcal mol^{-1}, respectively,[11] and the enthalpy of reaction derived above, we can calculate the heat of formation of HO_2, $\Delta H_{f,298K}(HO_2) = (1.9 \pm 0.3)$ kcal mol^{-1}. The current NASA panel recommendation[11] of $\Delta H_{f,298K}(HO_2) = (3.3 \pm 0.8)$ kcal mol^{-1} is somewhat higher than the currently determined value although the error limits overlap. The currently determined value is also lower than that currently recommended by IUPAC[12] of $\Delta H_{f,298K}(HO_2) = 3.5$ kcal mol^{-1}.

The mechanism of reaction 1 has been the subject of some debate. It was postulated in an early theoretical study by Weissman et al.[21] that the large value and negative temperature dependence of the rate coefficient for reaction 1a seemed to be inconsistent with the reaction proceeding through a simple hydrogen abstraction mechanism. Their suggestion, which was subsequently supported by Phillips and Quelch,[22] was that the reaction could proceed through a stabilized intermediate of the form

$$\text{Cl} + \text{HO}_2 \rightleftharpoons [\text{HOO---Cl}]^{\ddagger} \rightleftharpoons [\text{HOOCl}]^* \qquad (35)$$

This mechanism invoked a four centered elimination from the HOOCl intermediate for HCl + O_2 formation. Both sets of authors hypothesized that the HOOCl intermediate might be stabilized under certain atmospheric and laboratory conditions. Conversely, Mozurkewich[23] argued that from his RRKM calculations on reaction 1 the energetics of the process favor H atom attack. By assuming that reaction 2a involved the HOOCl intermediate, the threshold energy for the process HOOCl → HCl + O_2 was calculated. Subsequently, the calculated rate coefficient for reaction 1a, assuming this HOOCl intermediate, was found to be too small by a factor of 4. Instead, Mozurkewich[23] hypothesized that a hydrogen-bonded intermediate might be responsible for the large value of k_{1a} although it was a very speculative hypothesis due to the absence of a permanent dipole moment in the Cl atom. More recently, a density functional characterization of the $HClO_2$ potential energy surface by Sumathi and Peyerimhoff[24] concluded that the kinetics of reaction 1 were determined predominantly by the H-atom abstraction pathway. They claimed that the large observed value for rate coefficient k_{1a} was almost certainly due to the formation of the hydrogen-bonded intermediate as had been proposed earlier by Mozurkewich.[23] Furthermore, this effect was also responsible for the observed negative temperature dependence of reaction 1a. They suggested that formation of HOOCl* can occur, but the only energetically accessible dissociation routes available to this adduct are reformation of the reactants. As the temperature is increased, the formation of OH + ClO via O−O bond dissociation is expected to become more competitive with HCl + O_2 formation via O−Cl bond dissociation, which is certainly in good qualitative agreement with the experimental results. Additionally, Sumathi and Peyerimhoff[24] determine a third path for the fate of reaction 1, namely that of singlet oxygen formation. The only experimental evidence available, from a study by Keyser et al.,[25] obtained an upper limit of 5×10^{-4} for the yield of $O_2(b^1\Sigma_g^+)$ at 298 K. HOOCl remains to be experimentally observed although Francisco et al.[26] calculated that intense infrared absorptions should occur at 1399 and 392 cm^{-1}.

In conclusion, we present the first measurements of the HCl product channel in addition to the first direct determination of the temperature dependence of k_{1a}. Both of these quantities are in good agreement with earlier indirect evaluations.[7] Furthermore, our findings for the OH product channel, k_1 and k_{1b}, are also in good agreement with the current evaluations[11,12] of kinetic data for use in stratospheric modeling which are based on the results of ref 7[11] or on the basis of refs 7 and 9.[12]

Acknowledgment. The research described in this article was performed at the Jet Propulsion Laboratory, California Institute of Technology under a contract with the National Aeronautics and Space Administration.

References and Notes

(1) Leu, M. T.; Demore, W. B. *Chem. Phys. Lett.* **1976**, *41*, 121.
(2) Poulet, G.; Le Bras, G.; Combourieu, J. *J. Chem. Phys.* **1978**, *69*, 767.
(3) Burrows, J. P.; Cliff, D. I.; Harris, G. W.; Thrush, B. A.; Wilkinson, J. P. T. *Proc. R. Soc. London, Ser. A* **1979**, *368*, 463.
(4) Cox, R. A. *Int. J. Chem. Kinet.* **1980**, *12*, 649.
(5) Cox, R. A.; Derwent, R. G. *J. Chem. Soc., Faraday Trans. 1* **1977**, *73*, 272.
(6) Cattell, F. C.; Cox, R. A. *J. Chem. Soc., Faraday Trans. 2* **1986**, *82*, 1413.
(7) Lee, Y. P.; Howard, C. J. *J. Chem. Phys.* **1982**, *77*, 756.
(8) Dobis, O.; Benson, S. W. *J. Am. Chem. Soc.* **1993**, *115*, 8798.
(9) Riffault, V.; Bedjanian, Y.; Le Bras, G. *Int. J. Chem. Kinet.* **2001**, *33*, 317.
(10) Hess, G. H. *Bull. Sci. Acad. Imp. Sci.* (*St. Petersburg*) **1840**, *8*, 257−272.
(11) Sander, S. P.; Finlayson-Pitts, B. J.; Friedl, R. R.; Golden, D. M.; Huie, R. E.; Kolb, C. E.; Kurylo, M. J.; Molina, M. J.; Moortgat, G. K.; Orkin, V. L.; Ravishankara, A. R. *Chemical Kinetics and Photochemical Data for Use in Atmospheric Studies*, Evaluation No. 14, JPL Publication 02-25, Jet Propulsion Laboratory, Pasadena, 2002 (http://jpldataeval.jpl.nasa.gov/).
(12) Atkinson, R.; Baulch, D. L.; Cox, R. A.; Crowley, J. N.; Hampson, R. F., Jr.; Hynes, R. G.; Jenkin, M. E.; Kerr, J. A.; Rossi, M. J.; Troe, J. IUPAC Subcommittee on Gas Kinetic Data Evaluation for Atmospheric Chemistry Web Version; http://www.iupac-kinetic.ch.cam.ac.uk (July 2004).
(13) Wang, J. J.; Keyser L. F. *J. Phys. Chem. A* **2001**, *105*, 6479.
(14) Keyser, L. F. *J. Phys. Chem.* **1988**, *92*, 1193.
(15) Herriott, D.; Kogelnik, H.; Kompfner, R. *Appl. Opt.* **1964**, *3*, 523.
(16) Altmann, J.; Baumgart, R.; Weitkamp, C. *Appl. Opt.* **1981**, *20*, 995.
(17) Marrero, T. R.; Mason, E. A. *J. Phys. Chem. Ref. Data* **1972**, *1*, 3.
(18) Wang, J. J.; Keyser L. F. *J. Phys. Chem. A* **1999**, *103*, 7460.
(19) Mallard, W. G.; Westley, F.; Herron, J. T.; Hampson, R. F.; Frizzell D. H. *NIST Chemical Kinetics Standard*; Reference Database 17, Version 7.0 (Web Version), Release 1.2. http://kinetics.nist.gov/.
(20) Wang, J. J.; Keyser L. F. *J. Phys. Chem. A* **2001**, *105*, 10544.
(21) Weissman, M.; Shum, L. G. S.; Heneghan, S. P.; Benson, S. W. *J. Phys. Chem.* **1981**, *85*, 2863.
(22) Phillips, D. H.; Quelch, G. E. *J. Phys. Chem.* **1996**, *100*, 11270.
(23) Mozurkewich, M. *J. Phys. Chem.* **1986**, *90*, 2216.
(24) Sumathi, R.; Peyerimhoff, S. D. *J. Phys. Chem. A* **1999**, *103*, 7515.
(25) Keyser, L. F.; Choo, K. Y.; Leu, M. T. *Int. J. Chem. Kinet.* **1985**, *17*, 1169.
(26) Francisco, J. S.; Sander, S. P.; Lee, T. J.; Rendell, A. P. *J. Phys. Chem.* **1994**, *98*, 5644.